

## Single- and double-vortex vector solitons in self-focusing nonlinear media

José R. Salgueiro and Yuri S. Kivshar

*Nonlinear Physics Centre, Research School of Physical Sciences and Engineering, Australian National University,  
Canberra ACT 0200, Australia*

(Received 21 June 2004; published 22 November 2004)

We study two-component spatial optical solitons carrying an angular momentum and propagating in a self-focusing saturable nonlinear medium. When one of the components is small, such vector solitons can be viewed as a self-trapped vortex beam that guides either the fundamental or first-order guided mode, and they are classified as single- and double-vortex vector solitons. For such composite vortex beams, we demonstrate that a large-amplitude guided mode can stabilize the ringlike vortex beam which usually decays due to azimuthal modulational instability. We identify different types of these vector vortex solitons and demonstrate both vortex bistability and mutual stabilization effect.

DOI: 10.1103/PhysRevE.70.056613

PACS number(s): 42.65.Tg, 05.45.Yv, 47.20.Ky

### I. INTRODUCTION

Vortices are fundamental localized objects which appear in many branches of physics [1]. In fluid mechanics, coherent structures in the form of vorticity filaments are central dynamical objects to understand most fluid flows and particularly fluid turbulence. More recently, the study of vortices in Bose-Einstein condensates revealed many intriguing properties of superfluids created by ultracold atoms [2]. Different types of vortices can also be found and identified in optics; one of the simplest objects of this kind is a *phase singularity* in an optical wave front which is associated with a phase dislocation carried by a diffracting optical beam [3,4].

In self-focusing saturable nonlinear media, optical vortices can exist as self-trapped ringlike optical beams with zero intensity at the center carrying a phase singularity [5]. However, due to the self-focusing nature of nonlinearity such ringlike vortex beams become unstable to azimuthal perturbations, and they decay into several fundamental optical solitons flying off the main ring [6]. This effect was observed experimentally in different nonlinear media, including the saturable Kerr-like nonlinear media, biased photorefractive crystals, and quadratic nonlinear crystals operating in the self-focusing regime (see details and references in Ref. [7]). There are known several ways to stabilize this azimuthal modulational instability, including the vortex stabilization in the presence of a large-amplitude beam guided by it [8], and the stabilizing effect of partial incoherence of light on the vortex [9].

When a self-trapped vortex beam guides a large-amplitude fundamental beam, it creates together with the guided beam a composite object in the form of a *vector soliton* [7]. Mutual coupling between the fundamental beam and the vortex-carrying beam can create different novel types of composite vector solitons carrying an angular momentum [10–12]. The properties of such vector vortex solitons can differ substantially from the properties of one-component scalar vortices and scalar solitons. In particular, the mutual coupling between the beams can modify dramatically the vortex properties and, in particular, can suppress the development of azimuthal instability [8].

In this paper, we analyze the existence, general properties, and stability of the vector vortex solitons in a self-focusing

saturable nonlinear medium. We study two types of such two-component composite vortex solitons, i.e., *single-vortex vector solitons* that can be considered as the vortex-induced waveguide that guides a fundamental mode, and *double-vortex vector solitons*, when the localized field is similar to the first-order guided mode, being a vortex beam by itself. For some of the cases, we demonstrate that a mutual incoherent coupling between the vortex waveguide and a large-amplitude guided mode it guides can provide a strong stabilizing mechanism for stable or quasistable two-component vortex solitons to exist in such media, in agreement with the recent observation [13] of the stabilizing mechanism of the mutual coupling between different components of the composite vortex beam.

### II. MODEL

In order to study the vector vortex solitons, we consider the interaction of two mutually incoherent optical beams propagating in a self-focusing nonlinear saturable medium. The evolution equations for two incoherently interacting beams can be presented in the following dimensionless form:

$$\begin{aligned}
 i \frac{\partial u}{\partial z} + \Delta_{\perp} u + \frac{(|u|^2 + \mu|v|^2)u}{1 + \sigma(|u|^2 + |v|^2)} &= 0, \\
 i \frac{\partial v}{\partial z} + \Delta_{\perp} v + \frac{(|v|^2 + \mu|u|^2)v}{1 + \sigma(|u|^2 + |v|^2)} &= 0,
 \end{aligned}
 \tag{1}$$

where  $u$  and  $v$  are the dimensionless amplitudes of the fields, the parameter  $\sigma$  characterizes the nonlinearity saturation effect, and the mutually incoherent interaction between the modes is described by the coupling parameter  $\mu$ . The spatial coordinate  $z$  is the beam propagation direction, and  $\Delta_{\perp}$  stands for the transversal part of the Laplace operator in the cylindrical coordinates, defined through the radial,  $r=(x^2 + y^2)^{1/2}$ , and angular,  $\phi=\tan^{-1}(y/x)$ , coordinates. Model (1) provides a straightforward generalization to a number of important cases studied earlier. In particular, the limit  $\sigma \rightarrow 0$  corresponds to the Kerr medium with cubic nonlinearity [12] where all self-trapped beams may undergo collapse instabil-

ity. The case of the saturable nonlinearity at  $\mu=1$  corresponds to the incoherent beam interaction in photorefractive nonlinear media [10,11,14]. We look for stationary solutions of the system (1) that describe a radially symmetric single-charged vortex beam in the field  $u$ ,

$$u(r, \phi; z) = u(r)e^{i\phi}e^{iz}, \quad (2)$$

where the amplitude  $u(r)$  vanishes for  $r \rightarrow \infty$ . We assume that the vortex (2) guides (or is coupled to) the second beam,

$$v(r, \phi; z) = v(r)e^{il\phi}e^{i\beta z}, \quad (3)$$

where  $\beta$  is a dimensionless ratio of the propagation constants. In Eqs. (2) and (3) the functions  $u(r)$  and  $v(r)$  are the radial envelopes of the interacting fields, and  $l$  ( $l=0, \pm 1$ ) is an integer number related to the angular momentum that describes the number of phase windings of the guided mode. Equations for the stationary envelopes are given by

$$\begin{aligned} -u + \Delta_r u - \frac{1}{r^2}u + \frac{(u^2 + \mu v^2)u}{1 + \sigma(u^2 + v^2)} &= 0, \\ -\beta v + \Delta_r v - \frac{l^2}{r^2}v + \frac{(v^2 + \mu u^2)v}{1 + \sigma(u^2 + v^2)} &= 0, \end{aligned} \quad (4)$$

where  $\Delta_r$  is the radial part of the Laplace operator,

$$\Delta_r \equiv \frac{1}{r} \frac{d}{dr} \left( r \frac{d}{dr} \right).$$

The radially symmetric, spatially localized solutions of the system (4) describe different types of two-component composite solitons carrying an angular momentum, and they can form either single- or double-vortex vector solitons. In a two-dimensional geometry, such solutions can only be found numerically.

### III. SINGLE-VORTEX VECTOR SOLITONS

We consider the self-trapped vortex beam created in the main field  $u$ , with the asymptotic behavior  $u(r) \rightarrow 0$  as  $r \rightarrow \infty$ . Besides that, we require that the incoherently interacting component  $v(r)$  describes a localized mode, i.e.,  $v(r) \rightarrow 0$  and therefore  $\beta > 0$ . At the origin ( $r=0$ ), the boundary condition for the vortex is  $u=0$  and, if we seek the single-vortex solution with the fundamental guided mode ( $l=0$ ), the corresponding boundary condition for  $v(r)$  is  $dv/dr=0$  (or  $v=v_0$ ).

We find localized solutions numerically, by means of the relaxation technique. In Fig. 1, we show some examples of two-component localized solutions which describe a fundamental (no nodes) beam, guided by the self-trapped vortex that create together a *single-vortex vector soliton*. The existence domain for such solutions has been calculated numerically for a special case  $\sigma=0.5$ , and it is shown in Fig. 2 on the parameter plane  $(\beta, \mu)$ . The existence region for single-vortex vector solitons is composed of two regions which overlap in a triangular-shaped domain shaded with a different intensity in Fig. 1. In this intersection, two types of vortex solutions mark the familiar bistability phenomenon. The

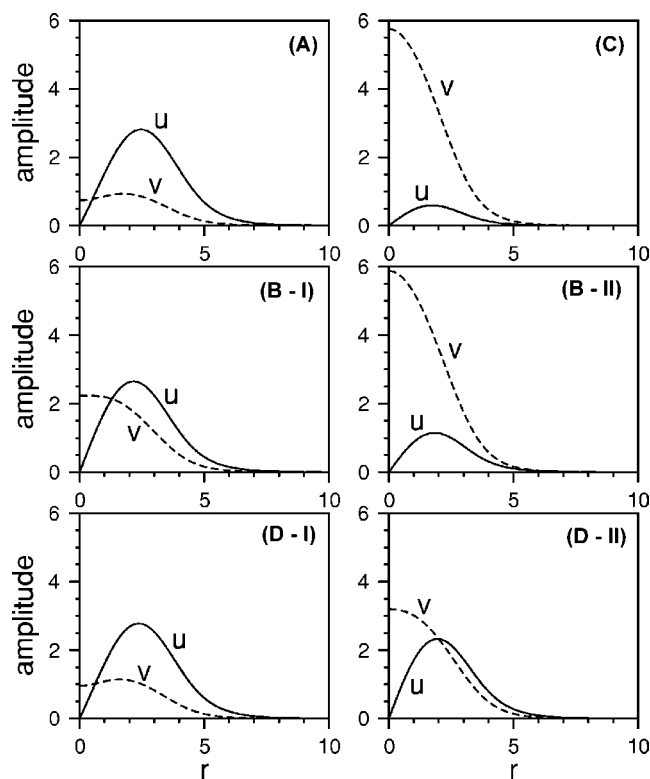


FIG. 1. Examples of single-vortex vector solitons created by the vortex beam  $u$  and the fundamental mode  $v$  it guides. Labels correspond to the points marked in Fig. 2. For points B and D, we show two different solutions named with roman numbers I and II, that exist due to bistability. The model parameters are: A ( $\mu = 1.10, \beta = 1.38$ ), B ( $\mu = 1.10, \beta = 1.44$ ), C ( $\mu = 1.17, \beta = 1.38$ ), and D ( $\mu = 1.17, \beta = 1.47$ ).

existence domain is restricted by the solid curves which describe some specific cutoff boundaries. Close to the lower cutoff, one of the components becomes small: the fundamental field in the left region (see the cases A and D-I), and the vortex in the right region (cases B-II and C). The other com-

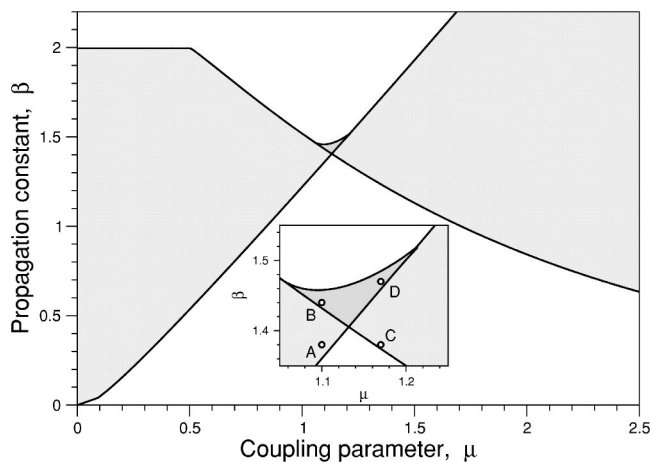


FIG. 2. Existence domain of the single-vortex vector solitons on the parameter plane  $(\beta, \mu)$  at  $\sigma=0.5$ . The inset shows an enlarged region of bistability where two different types of vortex-mode solutions coexist.

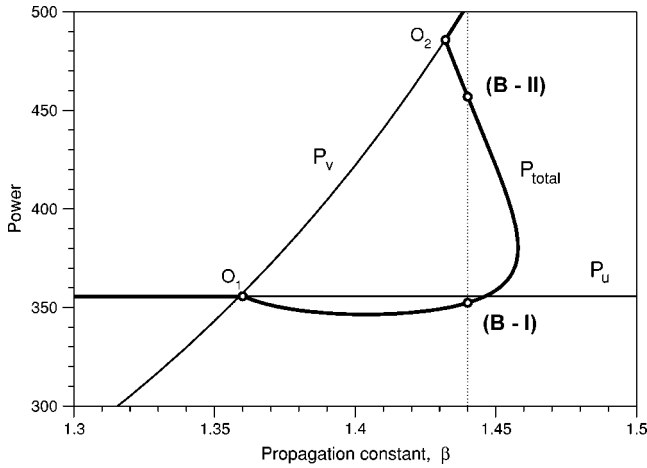


FIG. 3. Bifurcation diagram for the two-component vector vortex solitons, shown together with the families of the scalar fundamental and vortex solitons at  $\mu=1.1$ . Thin curves represent the powers  $P_u$  and  $P_v$  of each of the scalar solitons; the thick curve is the total power  $P_{\text{total}}$  of a composite vortex soliton. Points  $O_1$  and  $O_2$  are the bifurcation points where the vector soliton emerges, and the intersection points B-I and B-II correspond to the example of bistable single-vortex solutions for point B ( $\beta=1.44$ ) shown in Fig. 1.

ponent is therefore only weakly distorted. However, when the propagation constant  $\beta$  is close to the upper cutoff (cases B-I and D-II), the amplitudes of both components become comparable, affecting strongly each other. For small values of the coupling parameter  $\mu$ , the existence region is limited from above by the constant value  $1/\sigma$  (in our example,  $1/\sigma=2$ ), the value which can be easily explained by a simple qualitative analysis. Indeed, according to Eqs. (4), the existence of bounded stationary states for both  $u$  and  $v$  components requires the following conditions to be valid:

$$\max \left\{ \frac{u^2 + \mu v^2}{1 + \sigma(u^2 + v^2)} \right\} > 1, \quad (5)$$

$$\max \left\{ \frac{v^2 + \mu u^2}{1 + \sigma(u^2 + v^2)} \right\} > \beta. \quad (6)$$

Considering  $\mu \rightarrow 0$ , we obtain from Eq. (6) that the existence of localized solution requires that

$$\beta < \max \left\{ \frac{v^2}{1 + \sigma(u^2 + v^2)} \right\}. \quad (7)$$

The right-hand-side term vanishes when the amplitude of the component  $v$  vanishes at the cutoff, but it approaches the value  $1/\sigma$  when the amplitude of the field  $v$  becomes large. This analysis is valid for any type of the guided mode.

In order to describe the bistable vector solitons, in Fig. 3 we display the bifurcation diagram of the two-component vortex-mode localized solutions, for the partial and total beam powers. Composite vortex-mode solitons presented by the power dependence  $P_{\text{total}}$  originate at the bifurcation point  $O_1$  where the mode  $v$  is small and can be described by the linear theory. For larger value of  $\beta$ , this curve bends, and

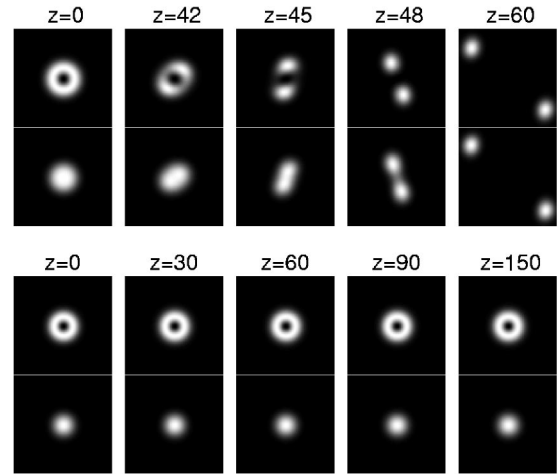


FIG. 4. Examples of the vortex propagation dynamics in the bistability domain. Shown are the field intensity profiles as gray-scale images at several propagation distances. Top: the components of the B-I vector soliton. Bottom: the components of the B-II vector soliton (see Figs. 1 and 3).

then it merges with the other partial power curve  $P_v$  at the bifurcation point  $O_2$  (see Fig. 3). The bistable solutions B-I and B-II, which are presented in Fig. 1 being related to point B in Fig. 2, correspond to a single value of the propagation constant  $\beta$  in the bistability domain. Importantly, two solutions have different stability properties, and only one of them is stable, as shown in Fig. 4. In general, the solutions belonging to the left region in the domain are unstable and those belonging to the right zone are stable.

The incoherent interaction between the vortex beam and the localized mode it guides has the character of attraction, and it may provide an effective physical mechanism for stabilizing the vortex beam in a self-focusing nonlinear medium. Indeed, a scalar vortex beam becomes unstable in a self-focusing nonlinear medium due to the azimuthal modulational instability. In this case, the vortex splits into the fundamental beams that fly off the main vortex ring. On the other hand, the bright solitons are known to be stable in such media. We expect that a mutual attraction of the components in a two-component beam may lead to a counterbalance of the vortex instability by the bright component when its amplitude is large enough. To confirm this idea, we consider a two-component composite structure consisting of a vortex beam together with the fundamental mode it guides, both described by Eqs. (1) at  $\mu=1.0$ . To study the mode stability, we propagate the stationary soliton solutions numerically. In Fig. 5, we compare the vortex breakup for the scalar and vector systems. In the top row, we show the propagation of a vortex alone in the scalar model; the vortex breaks up into two solitons which fly away after some distance. In the bottom row, we show the propagation of two coupled components (the vortex and bright mode it guides). Due to a strong incoherent coupling between the modes, the propagation of the vortex is stabilized for some propagation distances, so that the vortex breakup is delayed dramatically, as shown in Fig. 5 (lower row), or even become completely stable, similar to the case shown in Fig. 4 (low row). We confirm this

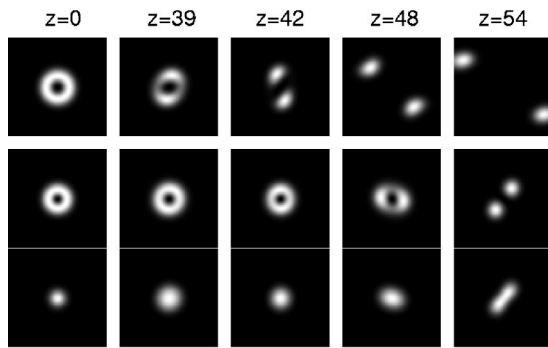


FIG. 5. Vortex stabilization due to mutual interaction. Shown are the field intensity profiles as gray-scale images at several propagation distances. Top: breakup of a scalar vortex soliton ( $v=0$ ). Bottom: both the vortex beam and the fundamental guided mode (approximated by a Gaussian beam) propagate together. Parameters are:  $\sigma=0.5$ ,  $\mu=1$ , and  $\beta=1.45$ .

stabilization mechanism by performing our study for a Gaussian input beam of the bright component instead of the exact stationary state, as would be easier realizing in experiment.

#### IV. DOUBLE-VORTEX VECTOR SOLITONS

To study types of vector vortex solitons, we consider the vortex beam in the field  $u$  coupled to the first-order guided mode described by the solution (3) with  $l=1$ . Thus for the field  $v$  we look for a vortexlike localized solution with the boundary condition  $v(r) \rightarrow 0$  at  $r=0$ . Our analysis shows that there exist four different kinds of such solutions, and they form the families of the so-called *double-vortex vector solitons*. We show some examples of these solutions in Fig. 6 and Fig. 8, whereas the existence domains for all solutions of this type are shown on the parameter plane ( $\beta, \mu$ ) in Fig. 7.

In the region labeled with number 5, there exist four types of localized double-vortex solutions, as shown for the point

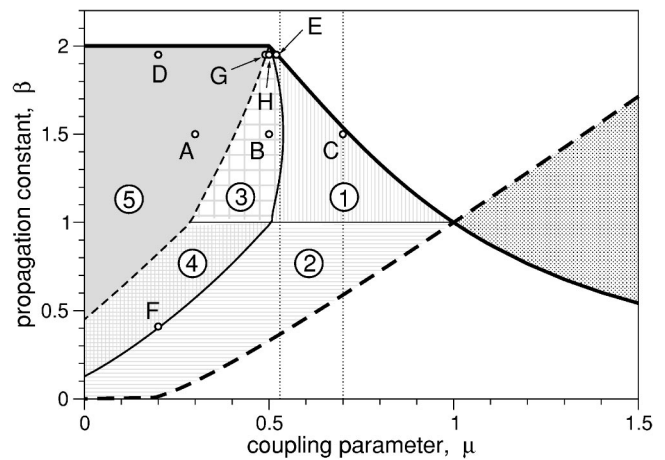


FIG. 7. Existence domain for different types of double-vortex solitons. Domain 1: only the solutions of type I; domain 2: only solution of type II; domain 3: solutions of types I, II, and III; domain 4: solutions of types I, II, and IV; domain 5: all four types of solutions exist. Two vertical thin dotted lines indicate the values of  $\mu$  for which the bifurcation diagrams are presented in Figs. 9 and 10.

A in Fig. 6. The first type (type I) is described by two rings where the ring in the field  $u$  is larger than the ring in the field  $v$ ; the opposite situation occurs for the solutions of type II (see Fig. 6). Other two types of solutions have one of the fields of a two-humped shape: either the field  $u$  (type III) or the field  $v$  (type IV). As the coupling parameter  $\mu$  grows, the valley in the two-humped solutions becomes shallower, and it disappears when the solution crosses a thin dashed line on the existence plane (Fig. 7), moving either to the domains 3 or 4. In the upper domain ( $\beta > 1$ , domain 3), no solution of type IV can be found further up from this line, being consequently the boundary of its existence domain. Besides, the solution of type III degenerates in a single-humped solution and still exists up to the thin continuous line (see Fig. 8, case B-III). The opposite occurs in the lower domain ( $\beta < 1$ , do-

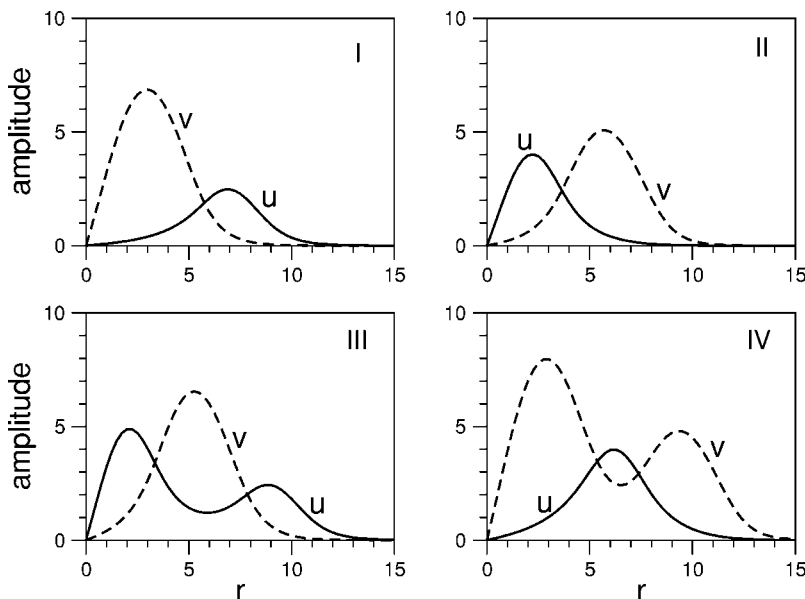


FIG. 6. Examples of four types of double-vortex vector solitons calculated for  $\sigma=0.5$ ,  $\mu=0.3$ , and  $\beta=1.5$ . All solutions correspond to point A in Fig. 7.

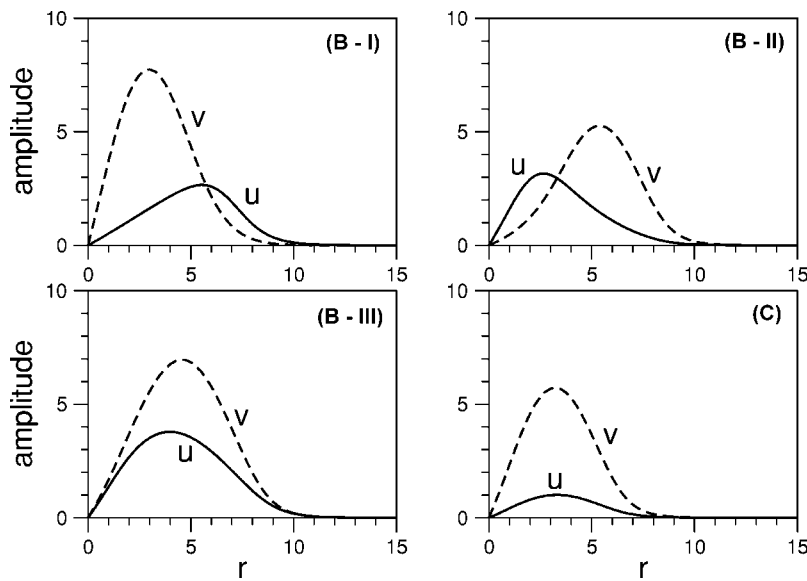


FIG. 8. Tristable solution found for  $\mu=0.5$  and  $\beta=1.5$  (point B in Fig. 7) and the unique solution found for  $\mu=0.7$  and  $\beta=1.5$  (point C). In all cases  $\sigma=0.5$ .

main 4), where the solitons of type III cannot be found to the right of the dashed line, and the solitons of type IV degenerate into single-humped modes.

Single-humped solutions of types I and II both exist up to the continuous thin line, though the maxima of both fields  $u(r)$  and  $v(r)$  are shifted, approaching each other as the parameter  $\mu$  increases (see the examples B-I and B-II in Fig. 8). Further up from this line, in the upper domain ( $\beta > 1$ , domain 1) the solutions II no longer exist, while the solutions I have a symmetric shape where the maxima of the fields approximately coincide (Fig. 8, case C). Dashed thick curve corresponds to the cutoff for such solutions, towards which the amplitude of the mode  $v$  becomes small and does not influence the vortex mode in the field  $u$ . On the other hand, the continuous thick line is the upper cutoff where a vector soliton originates.

Shape of these solutions can be explained qualitatively by a simple analysis. In fact, from Eq. (5), assuming  $\mu$  small and the maximum amplitude of  $v(r)$  much larger than that of  $u(r)$  (i.e., the parameter  $\beta$  close to the upper cutoff), we obtain the condition  $\max[u^2/(1+\sigma v^2)] > 1$ . Since  $v$  has a

larger maximum, the former condition cannot be satisfied unless the value of  $v$  is small at the position of the maximum of  $u$ , so that there still exists an effective potential with a relative maximum higher than 1. That requires that both fields have maxima shifted enough to each other, explaining the shape of the solutions in region 5 of Fig. 7. When  $\mu$  is larger, however, this condition can be satisfied when the maxima of both solutions almost coincide. Because the field  $v$  becomes self-guided and the shifting is not possible (due to the coupling between both components), each field has to be localized in the region close to the other. This explains the behavior of the solutions when  $\mu$  grows and the solution crosses the boundaries between region 5 and region 3, and then moves to region 1. On the other hand, if  $\beta$  is decreased, the component  $v(r)$  becomes smaller being guided by the component  $u(r)$ . This explains the behavior of the solutions

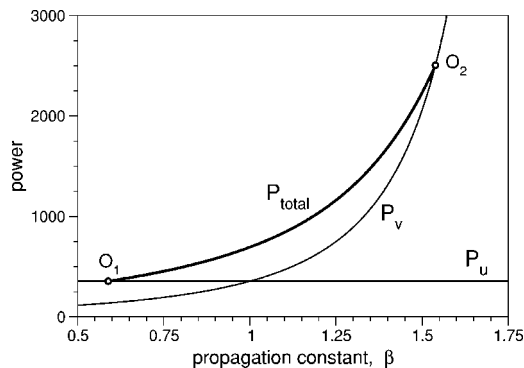


FIG. 9. Bifurcation diagram for vector and scalar vortex solitons (at  $\mu=0.7$ ).  $P_u$  and  $P_v$  (thin lines) are the powers of scalar vortices created in each component separately, while  $P_{total}$  (thick line) is the power of the vector soliton originated at the bifurcation points  $O_1$  and  $O_2$ .

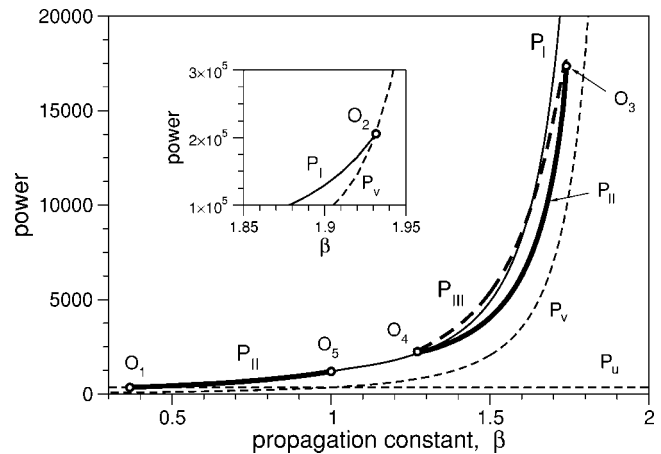


FIG. 10. Bifurcation diagram for vector and scalar vortex solitons (at  $\mu=0.53$ ).  $P_u$  and  $P_v$  (dashed thin lines) are the powers of the scalar vortices created in each component separately. Other curves are labeled with a subscript corresponding to different types of vector solitons: type I (continuous thin line), type II (continuous thick line), and type III (dashed thick line). Points  $O_1$  and  $O_2$  are bifurcation points, and  $O_3$ ,  $O_4$ , and  $O_5$  are critical points. An area near the bifurcation point  $O_2$  is shown in the inset.

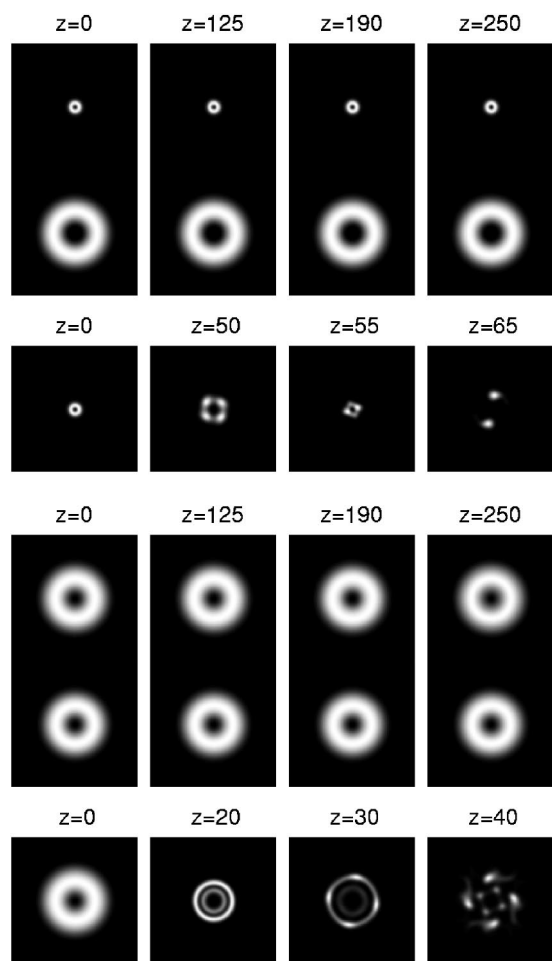


FIG. 11. Evolution of two types of stable double-vortex vector solitons corresponding to point D (type II, top rows) and point E (type I, bottom rows). For each soliton, both components are shown for different values of the propagation distance. For comparison, we show the corresponding unstable evolution when the component  $v$  is removed at the input.

crossing the boundaries from region 5 into region 4 and to region 2.

Existence of different kinds of double-vortex vector solitons leads to multistability phenomena as well as more complicated bifurcation diagrams. In Figs. 9 and 10, we present two examples of the bifurcation diagrams for two different values of the coupling parameter. In the first case, at  $\mu = 0.7$ , only one solution for each value of the propagation constant exists. At  $\beta = 1$ , both solutions of type I ( $\beta > 1$ , region 1 in Fig. 7) and type II ( $\beta < 1$ , region 2) merge together. In fact, for  $\beta = 1$ , it is deduced from Eqs. (4) that both solutions  $u(r)$  and  $v(r)$  become identical.

For smaller values of  $\mu$ , however, the existence of different kinds of vortex solutions generate a variety of branches in the bifurcation diagram, as shown in Fig. 10. In this case, there exist both the bifurcation points  $O_1$  and  $O_2$  and the critical points  $O_3$ ,  $O_4$ , and  $O_5$ , and three of the four kinds of solutions exist for some values of  $\beta$ . For other values of the coupling parameter  $\mu$ , different types of the bifurcation diagrams are obtained, and they all show a change of the solu-

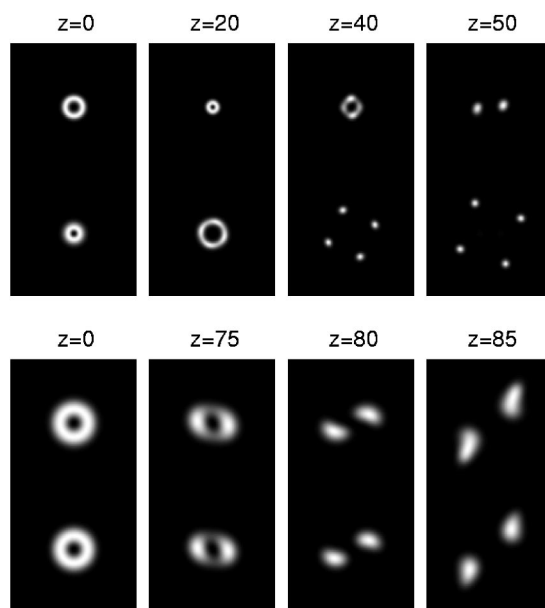


FIG. 12. Decay of the vortex vector solitons into 2+4 (top row) and 2+2 (bottom row) fundamental solitons. The upper case corresponds to the solution of type IV (point F;  $\mu = 0.2$ ,  $\beta = 1.41$ ), and the lower case to the solution of type I (point C;  $\mu = 0.7$ ,  $\beta = 1.5$ ).

tions when a boundary between different existence domains is crossed.

In Fig. 11, we show two examples of stable propagation. The top rows present the evolution of the vector soliton corresponding to point D in Fig. 7. For comparison, we show unstable propagation of the first component alone, when the second vortex component is removed from the input. In the latter case, the vortex decays after propagating for some distance while the two component soliton remains virtually stable for much longer propagation distance owing to the coupling between both the components. In general, it is possible to achieve a double-vortex vector soliton which remains stable for an arbitrary distance provided we chose a state close enough to the upper cutoff, where one of the components has larger amplitude and the interaction between both components is strong. In the bottom rows, we show another example of the stable propagation corresponding to point E in Fig. 7.

Different types of the double-vortex vector solitons demonstrate a rich variety of the instability-induced scenarios of their evolution. In Fig. 12 we present two examples of the vortex evolution with two characteristic scenarios of the vortex decay, producing either 2+4 (e.g., point F) or 2+2 (e.g., point C) fundamental solitons. Finally, in Fig. 13 we show two more complicated scenarios of the vortex instability to illustrate a variety of the patterns that can be observed. In the top row, where the input state corresponds to point G, the soliton decays in a complex way displaying a sequence of symmetric patterns. In the bottom row, where the input state corresponds to point H, the double-vortex soliton propagates in a quasistable way performing breathing radial oscillations. In all the cases discussed here, the topological charges of both the components are chosen with the same sign (+1).

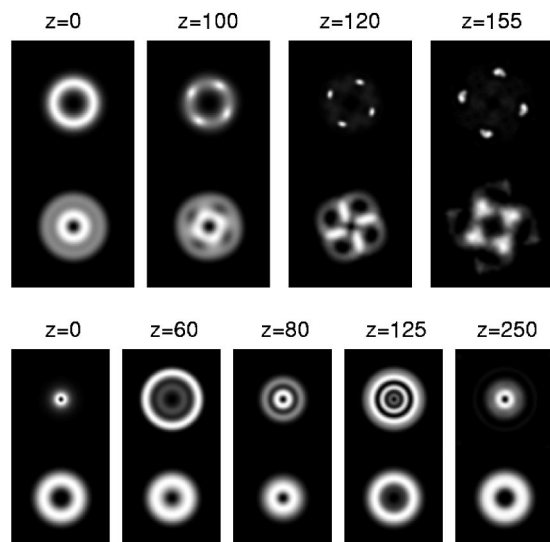


FIG. 13. Examples of the vortex instability scenarios. Top: decay of type IV vortex solitons corresponding to point G ( $\mu=0.49$ ,  $\beta=1.95$ ). Bottom: quasistable propagation of the vortex with breathing components for type II vector solitons (point H;  $\mu=0.5$ ,  $\beta=1.95$ ).

The case of the opposite charges has also been studied, and the similar evolution scenarios have been observed.

## V. CONCLUSIONS

We have analyzed the existence and basic properties of the two-component composite optical beams carrying an an-

gular momentum, the so-called vector vortex solitons. We have considered two major types of such solitons that propagate in self-focusing saturable nonlinear media and can be classified in the low-intensity limit through the fundamental and first-order localized modes guided by the main vortex beam. We have calculated the existence domains of such vortex composite solitons and studied numerically their stability to weak perturbations. In particular, we have revealed a different mechanism for stabilizing the vortex azimuthal modulational instability by a co-propagating guided mode of a large amplitude. We have demonstrated the existence of bistable composite double-vortex solitons as well as studied their instability-induced dynamics. We believe that similar results can be obtained for composite vortices in other types of nonlinear models describing the mutual coupling between several fields, and our results can be useful for other fields such as the physics of the multispecies Bose-Einstein condensates of ultracold atoms.

## ACKNOWLEDGMENTS

This work was partially supported by the Australian Research Council. J. R. Salgueiro acknowledges financial support from the Secretaría de Estado de Educación y Universidades of Spain supported by the European Social Fund, and he thanks Nonlinear Physics Center at the Research School of Physical Sciences and Engineering for warm hospitality during his stay in Canberra.

- 
- [1] L. M. Pismen, *Vortices in Nonlinear Fields* (Clarendon Press, Oxford, 1999).
  - [2] J. E. Williams and M. J. Holland, *Nature (London)* **401**, 586 (1999); K. W. Madison, F. Chevy, W. Wohlleben, and J. Dalibard, *Phys. Rev. Lett.* **84**, 806 (2000); C. Raman, J. R. Abo-Shaer, J. M. Vohels, and W. Ketterle, *ibid.* **87**, 210402 (2001).
  - [3] For a comprehensive review of optical vortices, see M. S. Soskin and M. V. Vasnetsov, in *Progress in Optics*, edited by E. Wolf (Elsevier, Amsterdam, 2001), Vol. 42.
  - [4] For a comprehensive source of references, see G. A. Swartzlander, Jr., *Singular Optics/Optical Vortex References*, <http://www.u.arizona.edu/grovers/SO/so.html>
  - [5] Such beams were suggested in V. I. Kruglov and R. A. Vlasov, *Phys. Lett.* **111A**, 401 (1985).
  - [6] W. J. Firth and D. V. Skryabin, *Phys. Rev. Lett.* **79**, 2450 (1997); D. V. Skryabin and W. Firth, *Phys. Rev. E* **58**, 3916 (1998).
  - [7] Yu. S. Kivshar and G. P. Agrawal, *Optical Solitons: From Fibers to Photonic Crystals* (Academic, San Diego, 2003).
  - [8] J. Yang and D. E. Pelinovsky, *Phys. Rev. E* **67**, 016608 (2003).
  - [9] C. C. Jeng, M. Shih, K. Motzek, and Yu. Kivshar, *Phys. Rev. Lett.* **92**, 043904 (2004).
  - [10] Z. H. Musslimani, M. Segev, and D. N. Christodoulides, *Opt. Lett.* **25**, 61 (2000).
  - [11] Z. H. Musslimani, M. Segev, D. N. Christodoulides, and M. Soljacić, *Phys. Rev. Lett.* **84**, 1164 (2000).
  - [12] J. N. Malmberg, A. H. Carlsson, D. Anderson, M. Lisak, E. A. Ostrovskaya, and Yu. S. Kivshar, *Opt. Lett.* **25**, 643 (2000).
  - [13] Fangwei Ye, Jiandong Wang, Liangwei Dong, and Yong-Ping Li, *Opt. Commun.* **230**, 219 (2004).
  - [14] W. Krolikowski, G. McCarthy, Yu. S. Kivshar, C. Weillau, C. Denz, J. J. García-Ripoll, and V.M. Pérez-García, *Phys. Rev. E* **68**, 016612 (2003).